Molecular charge transport : relating orbital structures to the conductance properties

Guédon, C.M.

Citation

Guédon, C. M. (2012, November 6). *Molecular charge transport : relating orbital structures to the conductance properties*. *Casimir PhD Series*. Retrieved from https://hdl.handle.net/1887/20093

Cover Page

The handle http://hdl.handle.net/1887/20093 holds various files of this Leiden University dissertation.
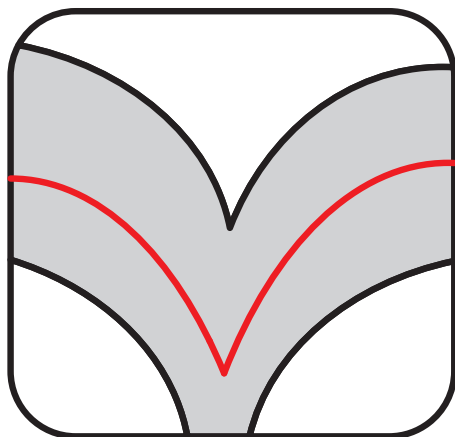
Author: Guédon, Constant Marcel
Title: Molecular charge transport : relating orbital structures to the conductance properties
Issue Date: 2012-11-06

6

Evidence for quantum interference in molecular charge transport

6.1 INTRODUCTION

As the dimensions of a conductor approach the nano-scale, quantum effects will begin to dominate its behavior. This entails the exciting possibility of controlling the conductance of a device by direct manipulation of the electron wave function. Such control has been most clearly demonstrated in mesoscopic semiconductor structures at low temperatures. Indeed, the Aharanov-Bohm effect[1], conductance quantization [2, 3] and universal conductance fluctuations [4] are direct manifestations of the electron wave nature. However, an extension of this concept to more practical temperatures has not been achieved so far. As molecules are nano-scale objects with typical energy level spacings ($\sim$ eV) much larger than the thermal energy at 300 K ($\approx$ 25 meV), they are natural candidates to enable such a break-through [5–11]. Fascinating phenomena including giant magnetoresistance, Kondo effects and conductance switching, have previously been demonstrated at the molecular level[12–18]. Here, we report direct evidence for destructive quantum interference in charge transport through two-terminal molecular junctions at room temperature. Furthermore, we show that the degree of interference can be controlled by simple chemical modifications of the molecule. Not only does this provide the experimental demonstration of a new phenomenon in quantum charge transport, it also opens the road for a new type of molecular devices based on chemical or electrostatic control of quantum interference.

The wave nature of electrons is fundamental to our understanding of almost all of chemistry. In fact, the very existence of molecular orbitals is a direct result of spatial confinement of electron waves. This in turn leads to pronounced reactivity variation at different sites of molecules. The electron wave character also plays a key role in mesoscopic physics, which studies quantum phenomena in charge transport. For example, the conductance properties of mesoscopic ring structures at low temperatures are dominated by quantum interference. If the partial waves through both branches of the ring add up destructively (constructively) a suppression (enhancement) of the conductance is observed. For certain classes of molecular junctions, a similar effect is expected [6–11]. However, in that case the picture of interference resulting from distinct spatial paths is no longer valid. Instead, interference in a molecule must be described in terms of electron propagation via paths of orbitals, differing not only in space, but also in energy. Since the properties of molecular orbitals can be manipulated by chemical design, quantum interference promises control over the conductance of molecular devices at the wave function level. In fact, conductance tuning over orders of magnitude at ambient temperatures comes within reach. Although

variations in charge transfer rates within donor-bridge-acceptor molecules can be explained in terms of interference [19, 20], only indirect indications for interference have been found in molecular conductance experiments [21, 22]. Here, we provide unambiguous evidence for destructive quantum interference in two-terminal molecular junctions.

6.2   EXPERIMENTAL DETAILS

To investigate the influence of quantum interference on molecular conductance properties, five rigid π-conjugated molecular wires are synthesized [1] (see capter 2). The first two molecules (AQ-MT and AQ-DT, left in figure 6.1 A) contain an anthraquinone-unit. This makes them cross-conjugated , note that linear conjugation refers to a sequence of alternating single and double bonds between both ends of an organic molecule [23, 24]. Cross-conjugation, however, implies that the sequence of alternating single and double bonds between both ends of the molecule is broken, although all C-atoms have formed double or triple bonds, i.e. all C-atoms are sp^2 or sp hybridized. The AQ-MT molecule is terminated by a protected thiol group at one side only (monothiolated: MT), whereas AQ-DT is dithiolated (DT). The third molecular wire (AC-DT) contains a central anthracene-unit and is linearly conjugated. Otherwise it is very similar to AQ-DT, e.g. both have a length of 24.5 Å. Finally, two linearly conjugated reference compounds, oligo(phenylene-ethynylene)-monothiol and -dithiol (OPE3-MT and OPE3-DT), are studied (see chapter 5). We stress that apart from the thiols, all five molecules have the same phenylene-ethynylene endgroups.

To measure transport, we first create self-assembled monolayers (SAMs) of each molecule on thin Au layers (200 nm, Si-substrates). To obtain high-quality, densely packed SAMs, we use a procedure established recently (Chapter 5) [25]. Next, a conducting atomic force microscopy (AFM) probe is brought in close contact to a SAM. In this way, we can perform charge transport experiments through the molecular layer, using the Au-covered substrate and the AFM-tip as electrodes (figure 6.1B). We typically connect to a few hundred molecules, while measuring current, I, versus bias voltage V [26]. However, the exact number does vary. For this reason, we present our results in two-dimensional (2D) histograms. Figure 6.1 C shows such a 2D-histogram for AC-DT. To construct this plot, we have logarithmically binned the dI/dV-values (determined numerically) for each bias applied (see chapter 5). This effectively results in a

[1]The molecules and the SAM are made by Hennie Valkenier and Kees Hummelen at the University of Groningen
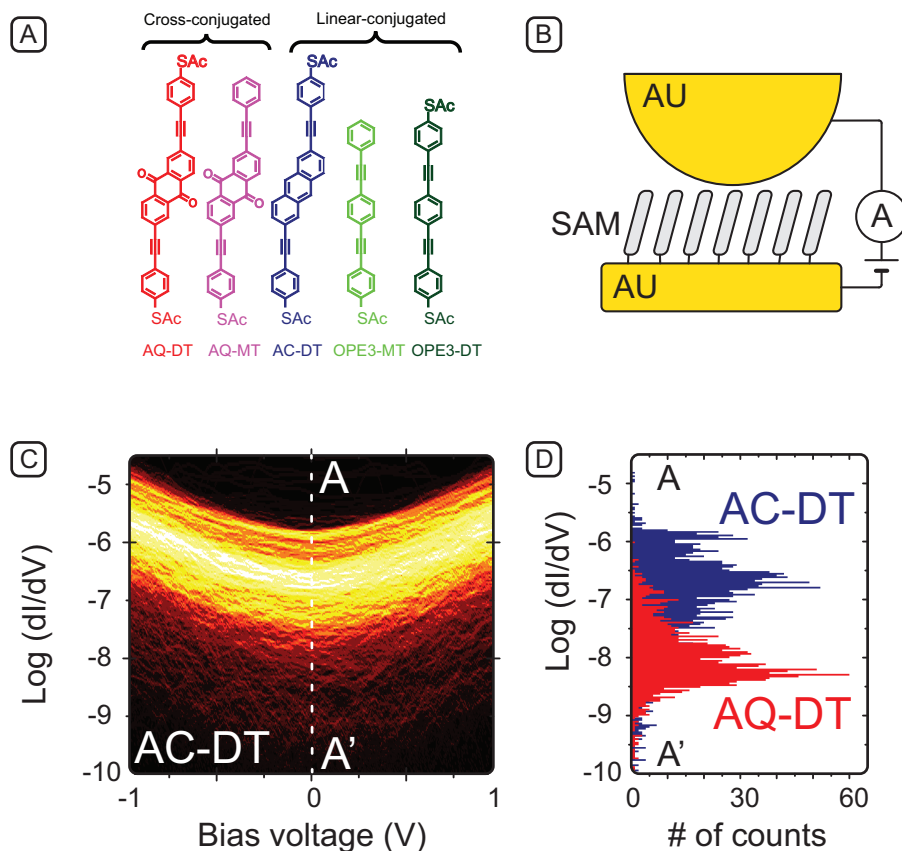
FIGURE 6.1: **Conductance measurements on molecular wires**. **A**, chemical structure of the molecules used. AQ-DT and AQ-MT are both cross-conjugated, whereas AC-DT, OPE3-DT and OPE3-MT are linearly conjugated. AQ-DT, AC-DT and OPE3-DT are dithiolated and thus symmetric; AQ-MT and OPE3-MT are monothiolated. The colour code is also used in the following figures. **B**, schematic view of the junction formed by the molecules self-assembled on a conducting substrate (Au) and the conducting AFM tip (Au), **C**, logarithmically binned 2D-histogram for the dI/dV-values vs. bias voltage V for AC-DT in Ω^{-1}, the colour scale indicates the number of counts (black: no counts; white: more than 40 counts) **D**, cross-section of the 2D-histogram shown in **C** along the line AA' (zero-bias conductance) resulting in a 1D-histogram (blue). Shown in red is the 1D-histogram for AQ-MT taken from Fig. 3a.

sequence of 1D-histograms, plotted for each V. To illustrate this, figure 6.1 D shows a cross-section of figure 6.1 C at $V = 0$ V (blue histogram; see dashed line in figure 6.1 C). This is the zero-bias 1D-histogram for AC-DT [27]. Representing our data in 2D-histograms has two major advantages. First, it allows us to show a full data set in one plot, without a need for either determining an average curve or for data selection [27]. For completeness: I(V)-curves that were either flat (no contact) or that showed direct contact are excluded from figure 6.1 and 6.3. However, such curves represent a small minority of our data ($\approx 5\%$). Second, it enables us to distinguish general tendencies in dI/dV-curves from statistical variations in the conductance values themselves. The latter are inherent to molecular transport studies [26, 27]. Figure 6.1-C clearly illustrates this advantage: a symmetric valley-like shape is seen for the full data range. This shape is virtually independent of the conductance values, which do scatter indeed (figure 6.1-D).

6.3 INDIRECT EVIDENCE FOR INTERFERENCES

Figure 6.1-D compares the zero-bias conductance histograms for both AQ-DT (red) and AC-DT (blue). Interestingly, AQ-DT exhibits conductance values that are almost two orders of magnitude lower than those of AC-DT. This is quite remarkable, since the energy difference between the HOMO and LUMO levels is very similar for these molecules (HOMO: highest occupied molecular orbital; LUMO: lowest unoccupied molecular orbital). From UV-Vis measurements, we find an optical HOMO-LUMO gap of 2.88 eV for AQ-DT and 2.90 eV for AC-DT. Our calculations yield fundamental HOMO-LUMO gaps of 4.23 eV and 4.61 eV, respectively [2]. Note that the optical gap and the fundamental gap differ by the electron-hole interaction. Furthermore, figure 6.1-D cannot be trivially explained from a weaker coupling of AQ-DT to the AFM-tip, since the endgroups of both molecules are exactly the same. As we shall elaborate on below, the large difference in conductance is instead indicative of destructive interference in the AQ-DT junctions. In figure 6.2-A we present calculations of the energy-dependent transmission function, $T(E)$, for junctions containing AC-DT, AQ-DT, and AQ-MT. This function describes the quantum mechanical probability that an electron with energy E traverses the molecular junction. Once $T(E)$ is known, the $I(V)$-curves can be calculated using Landauer's formula (Appendix C). In particular, the low bias conductance is given by $dI/dV(V = 0) = 2e^2/h \cdot T(E = E_F)$. For a molecular junction, $T(E)$ typically ex-

---

[2]The calculations are performed by Troels Markussen and Kristian Thygesen at the Danish Technical University in Copenhagen

hibits peaks around the orbital energies, where electrons can tunnel resonantly. In the energy gaps, $T(E)$ is normally rather featureless, as exemplified by AC-DT in figure 6.2-A. However, for AQ-DT and AQ-MT, $T(E)$ exhibits a strong dip or 'anti-resonance'. This feature is a result of a Fano-like [28, 29] destructive interference [6–11]. To reveal the origin of the anti-resonance, we transform the frontier molecular orbitals into an equivalent set of maximally localized molecular orbitals (LMOs)[9]. The upper part of figure 6.2-D shows the three relevant LMOs obtained for AQ-DT. Two are localized on the left and right parts of AQ-DT, respectively. These LMOs have the same energy and correspond essentially to the sum and difference of the almost degenerate HOMO and HOMO-1 (figure 6.2-A). The LMO localized in the center of AQ-DT is essentially the LUMO and has a higher energy. It is now clear that an electron with an energy, E, lying inside the HOMO-LUMO gap can traverse the molecule via two distinct paths: either directly from the left to the right LMO or by going via the energetically higher LMO (arrows in figure 6.2-D). It can be shown that the upper and lower routes yield a phase difference of π within the HOMO-LUMO gap, i.e., the partial waves interfere destructively (Appendix C). Consequently, $T(E)$ shows a strong minimum at the energy where the partial waves have equal weight. Figure 6.2-C illustrates this, by showing $T(E)$ calculated for the lower and upper routes separately, as well as for the combined three-site model. Note the similarity to figure 6.2-A. For AC-DT, the HOMO is well separated from the HOMO-1. Hence, a transformation to LMOs leads to only two, left and right localized, orbitals (figure 6.2-B). As there is only a single path available, no interference effects occur for AC-DT.

Note that quantum interference is only possible if the processes are phase coherent, so one may wonder if it is possible to observe this phenomenon at room temperature? First of all it is known in organic chemistry that the para- and meta- substitutions are responsible for different reactivities for reactions at room temperature, which is related to interferences. This is also found in room temperature transport measurements with molecules including para or meta connections on a phenyl ring [21, 30]. Moreover calculations predict that decoherence effects induced by electron-phonon interaction due to the finite temperature do not destroy the destructive interference in model cross-conjugated systems at room temperature [31–33]. One intuitive explanation is that we are in the strong coupling regime (see chapter 1) meaning that the electron residence time on the electronic levels is too short to interact with the phonons. Alternatively the distance needed over which the electron should be phase coherent is limited to the central part of the quinone moiety (or the phenyl ring in the para/meta case).

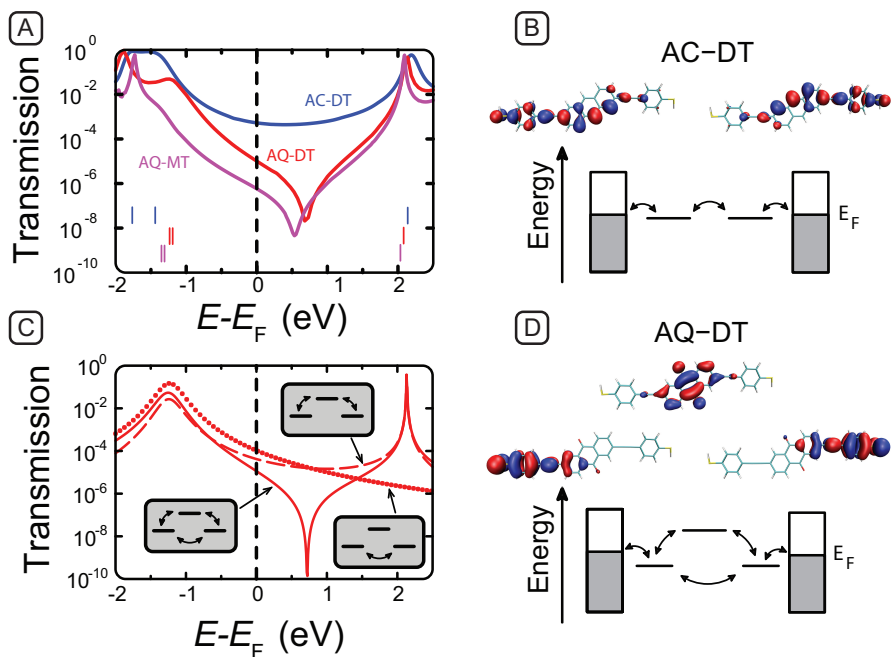We now compare the calculations with the experiments in figure 6.1-D. In

6

FIGURE 6.2: **Origin of interference in cross-conjugated molecules**. **A**, Transmission functions $T(E)$ for AC-DT (blue), AQ-DT (red) and AQ-MT (purple) calculated with DFT+Σ. The vertical bars mark the energies of the frontier orbitals HOMO-1, HOMO (left side) and LUMO (right side). The lower part of **B** and **D** pictures schematic transport models derived from the localized molecular orbitals presented in the upper parts. In the three-site model shown in **D**, there are evidently two routes through the molecule: a lower route directly from the left to the right site and an upper route via the central orbital. Panel **C** shows $T(E)$ for the lower (dotted line) and upper route (dashed line). A coherent addition of the transmission probability amplitudes from the two paths, with a phase difference of π, yields the three-site transmission function (solid line). This reproduces the essential features of **A**, for AQ-DT and AQ-MT..

figure 6.2-A, the $T(E_F)$-values are around two orders of magnitude lower for AQ-DT than for AC-DT. This is in reasonable agreement with the strongly reduced conductance values for AQ-DT in figure 6.1-D. We thus have a first, indirect evidence for interference in AQ-DT.

6.4 DIRECT EVIDENCE FOR QUANTUM INTERFERENCE

To investigate this further, we inspect the full 2D-histogram of AQ-DT (figure 6.3-A). For the full voltage range, its dI/dV-values are dramatically lower than those of AC-DT (figure 6.1-C). However, the 2D-histogram has a parabola-like appearance similar to AC-DT, i.e. we observe no anomaly that can be connected to the calculated transmission dip. Hence, although the surprisingly low conductance of AQ-DT is most likely due to quantum interference, the evidence is only indirect. This situation is comparable to the one in Refs. [21, 22]

Let us next consider AQ-MT molecules, which should also exhibit an anti-resonance (figure 6.2-A). Figure 6.3-B shows the 2D-histogram of the dI/dV-curves for AQ-MT. Remarkably, these data do show a clear anomaly at zero bias voltage. In particular, the curvature of the dI/dV-traces in figure 6.3 B is negative for all V (except around $V = 0$). What is equally striking in figure 6.3-B is the large voltage range over which the anomaly extends. Even up to $V = \pm 1$ V, the dI/dV-curves are dominated by the minimum at $V = 0$ V. This points to a characteristic energy scale of ≈ 1 eV, which corresponds well with the width of the interference-induced dip in $T(E)$ in figure 6.2-A. Moreover, this large energy scale rules out Kondo effects and Coulomb blockade as possible explanations for the anomaly. Coulomb blockade can also be ruled out via the experimental data. If Coulomb blockade were the dominant effect behind figure 6.3-B, it should also be present in the other molecular junctions, which have the same length and hence lead to roughly the same capacitance. However, no anomaly is seen in figures 6.1-C and 6.3-A, 6.3-C and 6.3-D. Hence, figure 6.3-B makes a strong case for quantum interference.

To further validate this interpretation, we calculate dI/dV-curves for AQ-MT from $T(E)$ (see Appendix C). A key role in these calculations is played by the position of the anti-resonance in $T(E)$ relative to E_F. This position is difficult to predict theoretically. This is related to the well-known problems of the applied methodology to describe energy level alignments and to the uncertainty of the size of the surface dipoles in the experiments. At Au-S interfaces, charge is transferred from Au to S, thus creating a surface dipole that shifts the molecular levels upward in energy. This shift depends, among other factors, on the
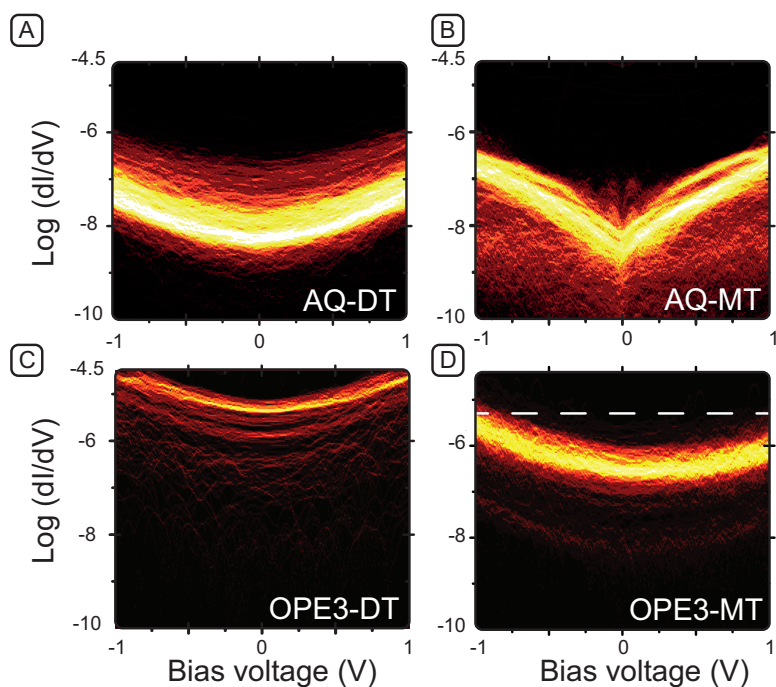
FIGURE 6.3: **Two-dimensional conductance histograms**. **A-D** show logarithmically binned 2D-histograms of dI/dV (in Ω^{-1}) vs. bias voltage V for AQ-DT (**A**), AQ-MT (**B**), OPE3-DT (**C**) and OPE3-MT (**D**). The colour scale indicates the number of counts and ranges from black (0 counts) to white (more than 40 counts). In **D**, a dashed line visualizes the asymmetry in the dI/dV-curves of OPE3-MT, resulting from asymmetric coupling. The corresponding molecular structures can be found in figure 6.1 a.
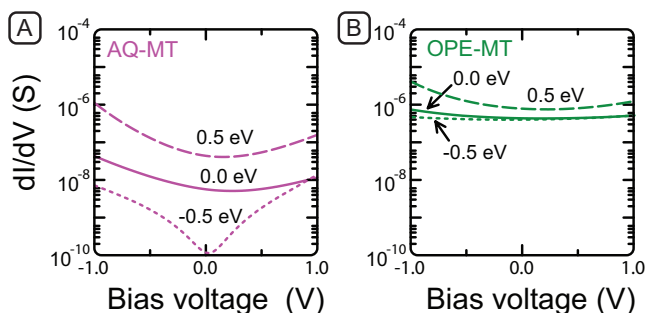
FIGURE 6.4: **Calculated dI/dV-curves for AQ-MT and OPE3-MT. A**, dI/dV for AQ-MT as computed from the transmission function in Fig. 2a. $T(E)$ was shifted by $\Delta E = 0.0$ eV, $\Delta E = 0.5$ eV and $\Delta E = -0.5$ eV, relative to E_F. We include asymmetry in the bias drop through a parameter $\eta = 0.6$ (Appendix C). To account for multiple molecules contacting the AFM-tip, we have multiplied the transmission function by a factor of 100. For $\Delta E = -0.5$ eV both the shape and the range of dI/dV, spanning two orders of magnitude, are in excellent agreement with the experiments (figure 6.3-B). **B**, Similar calculation for OPE3-MT. Asymmetric curves and higher conductance values with smaller variation are found, consistent with figure 6.3-D

surface density of molecules. The position of the anti-resonance is particularly sensitive to such effects due to the low density of states in the HOMO-LUMO gap. The computational limitation is illustrated best by comparing our calculations on AQ-DT (figure 6.2) with those in reference [22] (figure 5). In our figure 6.2, the anti-resonance lies to the right of E_F, whereas in reference [22], it lies to the left. It is thus reasonable to treat the position of the transmission minimum as a free variable within a limited energy window. In figure 6.4-A, we display dI/dV-curves for AQ-MT, calculated for three cases: no energy shift (compared to figure 6.2-A) and shifts of ± 0.5 eV. We take into account that AQ-MT molecules are probed asymmetrically. For a shift of -0.5 eV, the calculated dI/dV-characteristic is in remarkable agreement with the measured curves in figure 6.3 B. First, the V-like shape with negative curvature is reproduced. Second, the voltage scale and the range of dI/dV-values over which the minimum extends agree. Finally, the dI/dV-curves are nearly symmetric in both calculation and experiment. The latter is indeed noteworthy, since AQ-MT is contacted asymmetrically. The symmetry in figure 6.3-B must therefore be a consequence of $T(E)$ being symmetric around E_F or, equivalently, of E_F laying near the interference minimum. To independently confirm that monothiols are asymmetrically coupled, we measured dI/dV-curves for OPE3-DT (figure 6.3-C) and OPE3-MT (figure 6.3-D). As expected, symmetric data are obtained for OPE3-DT, whereas asymmetric dI/dV-curves are found for OPE3-MT (see

figure 6.4-B for calculations). Moreover in reference [34], Kim and co-workers observed linear I(V) curves around zero bias for oligoacene molecules (similar to the central part of ACDT) for both mono- and di-thiols which results in a parabolic shaped dI/dV as shown above. This reinforces the idea that the observed dip in the dI/dV is not caused by the monothiolated character of the molecules but truly a characteristic of the AQ molecules. Hence, we conclude that figure 6.3-B constitutes direct evidence for quantum interference in AQ-MT molecular junctions.

There is still the question why AQ-DT does not show a V-shaped dI/dV-curve, while its conductance is strongly suppressed. This is explained by the fact that AQ-DT junctions comprise two Au-S dipoles, whereas AQ-MT junctions have only one. Hence, in AQ-DT, the transmission dip is shifted to higher energies than in AQ-MT, i.e. it lies above E_F. In that case, no anomaly shows up in dI/dV-curves (see figure 6.4-A and Appendix C). Note that a higher energetic position of the dip of AQ-DT, compared to AQ-MT, is also predicted by our calculations (figure 6.2-A).

Now that we have direct evidence for quantum interference, the question should be asked what is needed for a full proof. One of the experiments that comes into mind is the use of a three-terminal junction set-up. Indeed the extra electrode, the gate, could be used to shift the molecular levels and so also move the interference dip in the transmission relative to the Fermi level. Indeed we have seen above that the relative position of the interference dip in the transmission function and the Fermi level are essential for the observation of the dip in the dI/dV. In this way we could show that when the levels are shifted for AQ-MT for example the characteristic dip in the dI/dV disappears. Inversely we could move the dip of AQ-DT closer to the Fermi level to make the dip in the dI/dV appear.

A second possible experiment is to look at the thermoelectric signature of the destructive interferences. Indeed by applying a temperature gradient, ΔT, between two electrodes contacting molecular species one can measure the obtained thermo-voltage, ΔV_{thermo}[35]. It has been shown that the Seebeck coefficient, $S = \Delta V_{thermo}/\Delta T$ is proportional to the slope of the transmission function at the Fermi level as shown in equation 6.1.

$$S = -\frac{\pi^2 k_B^2 T}{3e} \frac{\partial \ln(T(E))}{\partial E}\bigg|_{E=E_F} \tag{6.1}$$

As we can see in figure 6.5, we can relate the position and the sign of the Seebeck coefficient to the position of the Fermi level. For positive S, the Fermi level is located at the HOMO side of the transmission, oppositely for negative S, E_F
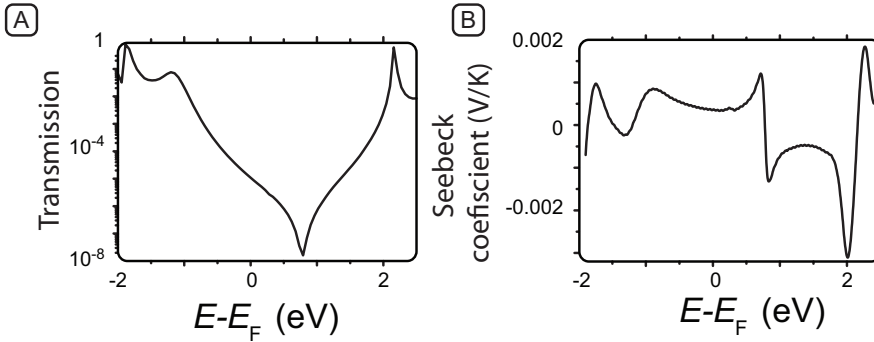
FIGURE 6.5: **Calculated transmission probability curves and Seebeck coefficient for AQ-DT. A**,transmission curves for AQ-DT calculated by DFT+Σ **B**, Corresponding Seebeck coefficient. All calculations are performed by Troels Markussen from the Danish technical university.

is located at the LUMO side of the transmission. The value of the measured S does determine the distance to the dip. Thermoelectric measurements make the determination of the Fermi level position possible.

Finally, we note that a magnetic field can not be practically used to manipulate the phase of the electrons and hence the interference.

6

6.5   CONCLUSIONS

In summary, our charge transport data on cross-conjugated anthraquinone derivatives are fully consistent with destructive interference in molecular junctions. The interference effects are intimately linked to the shapes and energies of the molecular orbitals and can thus be controlled by chemical design. The fact that interference in molecules is present at room temperature opens the road to a new type of molecular devices. Specifically, these include interference controlled molecular switches with very large on-off ratios[18, 23] and novel thermoelectric devices, with thermopower values tunable in magnitude and sign[36].

REFERENCES

[1] R. A. Webb, S. Washburn, C. P. Umbach, and R. B. Laibowitz, *Observation of h/e Aharonov-Bohm Oscillations In Normal-metal Rings*, Physical Review Letters **54**, 2696 (1985).

[2] B. J. van Wees, H. van Houten, C. W. J. Beenakker, J. G. Williamson, L. P. Kouwenhoven, D. van der Marel, and C. T. Foxon, *Quantized conductance of point contacts in a two-dimensional electron gas*, Physical Review Letters **60**, 848 (1988).

[3] D. A. Wharam, T. J. Thornton, R. Newbury, M. Pepper, H. Ahmed, J. E. F. Frost, D. G. Hasko, D. C. Peacock, D. A. Ritchie, and G. A. C. Jones, *One-dimensional transport and the quantisation of the ballistic resistance*, Journal of Physics C: Solid State Physics **21**, L209 (1988).

[4] C. W. J. Beenakker and H. van Houten, *Quantum Transport In Semiconductor Nanostructures*, Solid State Phys. **44**, 1 (1991).

[5] P. Sautet and C. Joachim, *Electronic interference produced by a benzene embedded in a polyacetylene chain*, Chemical Physics Letters **153**, 511 (1988).

[6] D. Q. Andrews, G. C. Solomon, R. P. Van Duyne, and M. A. Ratner, *Single Molecule Electronics: Increasing Dynamic Range and Switching Speed Using Cross-Conjugated Species*, Journal of the American Chemical Society **130**, 17309 (2008).

[7] C. A. Stafford, D. M. Cardamone, and S. Mazumdar, *The quantum interference effect transistor*, Nanotechnology **18**, 424014 (2007).

[8] M. Ernzerhof, M. Zhuang, and P. Rocheleau, *Side-chain effects in molecular electronic devices*, Journal of Chemical Physics **123** (2005), ISSN 0021-9606.

[9] T. Markussen, R. Stadler, and K. S. Thygesen, *The Relation between Structure and Quantum Interference in Single Molecule Junctions*, Nano Letters **10**, 4260 (2010).

[10] T. Markussen, J. Schiotz, and K. S. Thygesen, *Electrochemical control of quantum interference in anthraquinone-based molecular switches*, Journal of Chemical Physics **132**, 224104 (pages 6) (2010).

[11] G. C. Solomon, C. Herrmann, T. Hansen, V. Mujica, and M. A. Ratner, *Exploring local currents in molecular junctions*, Nature Chemistry **2**, 223 (2010).

[12] S. Schmaus, A. Bagrets, Y. Nahas, T. K. Yamada, A. Bork, M. Bowen, E. Beaurepaire, F. Evers, and W. Wulfhekel, *Giant magnetoresistance through a single molecule*, Nature Nanotechnology **6**, 185 (2011).

[13] R. H. M. Smit, Y. Noat, C. Untiedt, N. D. Lang, M. C. van Hemert, and J. M. van Ruitenbeek, *Measurement of the conductance of a hydrogen molecule*, Nature **419**, 906 (2002).

[14] S. Kubatkin, A. Danilov, M. Hjort, J. Cornil, J. L. Bredas, N. Stuhr-Hansen, P. Hedegard, and T. Bjornholm, *Single-electron transistor of a single organic molecule with access to several redox states*, Nature **425**, 698 (2003).

[15] L. Venkataraman, J. E. Klare, I. W. Tam, C. Nuckolls, M. S. Hybertsen, and M. L. Steigerwald, *Single-molecule circuits with well-defined molecular conductance*, Nano Letters **6**, 458 (2006).

[16] E. A. Osorio, K. O'Neill, M. Wegewijs, N. Stuhr-Hansen, J. Paaske, T. Bjornholm, and H. S. J. van der Zant, *Electronic excitations of a single molecule contacted in a three-terminal configuration*, Nano Letters **7**, 3336 (2007).

[17] A. Mishchenko, D. Vonlanthen, V. Meded, M. Burkle, C. Li, I. V. Pobelov, A. Bagrets, J. K. Viljas, F. Pauly, F. Evers, et al., *Influence of Conformation on Conductance of Biphenyl-Dithiol Single-Molecule Contacts*, Nano Letters **10**, 156 (2010).

[18] S. J. van der Molen and P. Liljeroth, *Charge transport through molecular switches*, Journal Of Physics-Condensed Matter **22**, 133001 (2010).

6

[19] C. Patoux, C. Coudret, J. P. Launay, C. Joachim, and A. Gourdon, *Topological effects on intramolecular electron transfer via quantum interference*, Inorganic Chemistry **36**, 5037 (1997).

[20] A. B. Ricks, G. C. Solomon, M. T. Colvin, A. M. Scott, K. Chen, M. A. Ratner, and M. R. Wasielewski, *Controlling Electron Transfer in Donor-Bridge-Acceptor Molecules Using Cross-Conjugated Bridges*, Journal of the American Chemical Society **132**, 15427 (2010).

[21] M. Mayor, H. B. Weber, J. Reichert, M. Elbing, C. von Hanisch, D. Beckmann, and M. Fischer, *Electric current through a molecular rod - Relevance of the position of the anchor groups*, Angewandte Chemie, International Edition **42**, 5834 (2003).

[22] D. Fracasso, H. Valkenier, J. C. Hummelen, G. C. Solomon, and R. C. Chiechi, *Evidence for Quantum Interference in SAMs of Arylethynylene Thiolates in Tunneling Junctions with Eutectic GaIn (EGaIn) Top-Contacts*, Journal of the American Chemical Society **133**, 9556 (2011).

[23] E. H. van Dijk, D. J. T. Myles, M. H. van der Veen, and J. C. Hummelen, *Synthesis and Properties of an Anthraquinone-Based Redox Switch for Molecular Electronics*, Organic Letters **8**, 2333 (2006).

[24] M. Gholami and R. R. Tykwinski, *Oligomeric and polymeric systems with a cross-conjugated pi-framework*, Chemical Reviews **106**, 4997 (2006).

[25] H. Valkenier, E. H. Huisman, P. A. van Hal, D. M. de Leeuw, R. C. Chiechi, and J. C. Hummelen, *Formation of High-Quality Self-Assembled Monolayers of Conjugated Dithiols on Gold: Base Matters*, Journal of the American Chemical Society **133**, 4930 (2011).

[26] D. J. Wold and C. D. Frisbie, *Fabrication and characterization of metal-molecule-metal junctions by conducting probe atomic force microscopy*, Journal of the American Chemical Society **123**, 5549 (2001).

[27] M. T. Gonzalez, S. M. Wu, R. Huber, S. J. van der Molen, C. Schonenberger, and M. Calame, *Electrical conductance of molecular junctions by a robust statistical analysis*, Nano Letters **6**, 2238 (2006).

[28] U. Fano, *Effects of Configuration Interaction on Intensities and Phase Shifts*, Physical Review **124**, 1866 (1961).

[29] A. E. Miroshnichenko, S. Flach, and Y. S. Kivshar, *Fano resonances in nanoscale structures*, Reviews Of Modern Physics **82**, 2257 (2010).

6

[30] S. J. van der Molen, J. Liao, T. Kudernac, J. S. Agustsson, L. Bernard, M. Calame, B. J. van Wees, B. L. Feringa, and C. Schoenenberger, *Light-Controlled Conductance Switching of Ordered Metal-Molecule-Metal Devices*, Nano Letters **9**, 76 (2009).

[31] R. H. Goldsmith, M. R. Wasielewski, and M. A. Ratner, *Electron transfer in multiply bridged donor-acceptor molecules: Dephasing and quantum coherence*, Journal Of Physical Chemistry B **110**, 20258 (2006).

[32] D. Q. Andrews, G. C. Solomon, R. H. Goldsmith, T. Hansen, M. R. Wasielewski, R. P. Van Duyne, and M. A. Ratner, *Quantum Interference: The Structural Dependence of Electron Transmission through Model Systems and Cross-Conjugated Molecules*, Journal Of Physical Chemistry C **112**, 16991 (2008).

[33] T. Markussen, private communications.

[34] B. Kim, S. H. Choi, X. Y. Zhu, and C. D. Frisbie, *Molecular tunnel junctions based on pi-conjugated oligoacene thiols and dithiols between ag, au, and pt contacts: effect of surface linking group and metal work function*, Journal Of The American Chemical Society **133**, 19864 (2011).

[35] R. Pramod, J. Sung-Yeon, R. A. Segalman, and A. Majumdar, *Thermoelectricity in molecular junctions*, Science **315**, 1568 (2007).

[36] J. P. Bergfield and C. A. Stafford, *Thermoelectric Signatures of Coherent Transport in Single-Molecule Heterojunctions*, Nano Letters **9**, 3072 (2009).

6